Photodiagnosis and Photodynamic Therapy 25 (2019) 480–491

Contents lists available at ScienceDirect

Photodiagnosis and Photodynamic Therapy

journal homepage: www.elsevier.com/locate/pdpdt

Folate-directed zinc (II) phthalocyanine loaded polymeric micelles engineered to generate reactive oxygen species for efficacious photodynamic therapy of cancer

Łukasz Lamch[a], Julita Kulbacka[b,*], Magda Dubińska-Magiera[c], Jolanta Saczko[b], Kazimiera A. Wilk[a,*]

[a] Department of Organic and Pharmaceutical Technology, Faculty of Chemistry, Wroclaw University of Science and Technology, Wybrzeże Wyspiańskiego 27, 50-370, Wroclaw, Poland
[b] Department of Molecular and Cellular Biology, Wroclaw Medical University, Borowska 211A, 50-556, Wroclaw, Poland
[c] Department of Animal Developmental Biology, Institute of Experimental Biology, University of Wroclaw, Sienkiewicza 21, 50-335, Wroclaw, Poland

ARTICLE INFO

Keywords:
Nanomedicine
Functionalized polymeric micelles
Biocompatible block copolymers
Photodynamic reaction
Reactive oxygen species
Cytoskeletal analysis
Metastatic melanoma
Resistant ovarian carcinoma

ABSTRACT

Targeted and effective drug transport is becoming an attractive option in cancer therapy since it can improve drug efficacy and reduce drugs' side effects in normal tissues. In addition to using specific surface ligand molecules, the selective drug delivery can be accomplished via enhanced permeability and retention effect. Therefore, in our studies, we entrapped zinc (II) phthalocyanine (ZnPc) – a second generation photosensitizer – in folate-functionalized micelles of the biocompatible, FDA-approved for biomedical application diblock copolymer methoxypoly(ethylene oxide)-b-poly(L-lactide) (mPEG-b-PLLA) and its derivative with folate (FA) attached to the end of PEG chain (FA-PEG-b-PLLA). Dynamic light scattering (DLS) measurements confirmed the micellar size to be < 150 nm in diameter, a low polydispersity index, and good colloid stability of the studied nanocarriers, while atomic force microscopy (AFM) was used to study their morphology. The application potential of the resulting micelles was evaluated in cyto- and photocytotoxicity studies in conjunction with intracellular distribution and accumulation imaging of the photosensitizer delivered to ovarian carcinoma (SKOV-3) and metastatic melanoma (Me45) cell lines. Reactive oxygen species generation study was performed after photodynamic reaction, and cellular cytoskeleton reorganization was visualized after undergoing a photodynamic reaction. The results demonstrated that the functionalized polymeric micelles are promising nanocarriers for photodynamic therapy procedures and can be used in anticancer drug delivery.

1. Introduction

Supramolecular assemblies fabricated from block copolymers, including their functionalized derivatives, have been receiving intensive attention as possible candidates for biomedical applications [1]. The most interesting aspect of polymeric micelles and other nanocarriers, especially in anticancer treatment, is that they can be modified with different biologically active functionalities [2,3]. These can be either covalently attached to the block copolymer chain [4] or incorporated through specific interactions [5]. This provides targeting of the active type, where ligands (including vitamins, aptamers, lectins, carbohydrates, affibodies, antibodies, and antibody fragments) are attached to the nanocarrier's surface for a selective drug or contrast agents delivery to specific cells [6]. This is in contrast to passive targeting, where it is the EPR (i.e. enhanced permeability and retention) effect that facilitates the accumulation of the drug in the tumor tissue region. Ligand-targeted therapies involve the application of the selected ligand that binds specifically to the receptor which is primarily overexpressed on cancer

Abbreviations: ZnPc, zinc (II) phthalocyanine; Ln, lanthanides; FA, folic acid; DDS, drug delivery systems; PM, polymeric micelle; DLS, dynamic light scattering; ROS, reactive oxygen species; AFM, atomic force microscopy; RES, reticuloendothelial system; TEM, transmission electron microscopy; PLA, polylactide; PCL, polycaprolactone; EE, endosomal environment; PGA, polyglycolide; PEG, polyethylene glycol; FR, folate receptor; PS, photosensitizer; SDS-PAGE, sodium dodecyl sulfate polyacrylamide gel electrophoresis; PBS, phosphate-buffered saline; TCA, trichloric acid; MTT, 3-(4,5-dimethylthiazol-2-yl)-2,5-diphenyltetrazolium; NMR, nuclear magnetic resonance; ABMDMA, 9,10-anthracenediyl-bis(methylene)dimalonic acid sodium salt; DCF, 2,7-dichlorofluorescein; CLSM, confocal laser scanning microscopy

* Corresponding authors.
E-mail addresses: julita.kulbacka@umed.wroc.pl (J. Kulbacka), kazimiera.wilk@pwr.edu.pl (K.A. Wilk).

https://doi.org/10.1016/j.pdpdt.2019.02.014
Received 13 January 2019; Received in revised form 8 February 2019; Accepted 11 February 2019
Available online 12 February 2019
1572-1000/

cells. This ligand, bounded to a therapeutic drug or its nanocarrier, can be used to deliver specifically the nonselective drug into a cancer cell [7]. Drug delivery systems contribute to an broadening of the therapeutic window range by increasing the delivery to the target tissue as well as the target to non-target tissue ratio. As a result, this leads to a reduction in the "minimum effective dose" of the drug and thus simultaneously lowers the concomitant drug toxicity, providing an improved therapeutic efficacy at equivalent concentrations in plasma [8]. Polymeric micelles possessing exceptional properties, such as an appropriate size (20–200 nm), high drug loading capacity, stability, long circulation in blood, selective accumulation in solid tumor, and the ability to escape from the reticuloendothelial system (RES) and renal exclusion, seem to be the most sophisticated nanosystems for clinical approaches and relevant research focusing on the enhanced transport of hydrophobic drugs, photosensitizers, and DNA, including functionalization by various cell-specific ligands [2,9,10].

Amphiphilic block copolymers with hydrophobic segment derived from aliphatic polyesters of hydroxyalkanoic acids, e.g. polylactide (PLA), polycaprolactone (PCL), and polyglycolide (PGA), are considered as biocompatible and biodegradable by hydrolytic enzymes under physiological conditions as well as by products approved by the FDA for clinical use [11]. Furthermore, the polymeric micelles prepared from the self-assembled poly(ethylene oxide) and poly(L-lactide) block copolymer exhibit architectures of the core-shell type, in which the biodegradable poly(L-lactide) segments can associate to form a core, making it possible to entrap hydrophobic drugs, and the polyethylene glycol (PEG) chains form a hydrophilic shell, enabling the nanocarrier to exhibit the "stealth effect" during its circulation in blood [12].

It is alleged that the folate receptor (FR) constitutes an extremely selective tumor marker overexpressed in more than 90% of ovarian carcinomas. Relatively increased expression of the FR was noticed in several types of human cancers (e.g. melanoma and ovarian cancer). Interestingly, the receptor is generally not present in most normal tissues, excluding choroid plexus and placenta, and has low levels in lungs, thyroid, and kidney [8]. Folic acid (FA), as the targeting ligand, is very beneficial regarding its storage stability, low toxicity and immunogenicity, low molecular weight (M_W of 441 Da), biocompatibility, high affinity for the FR ($K_d = 10^{-10}$ M), and low cost [13]. The FA-based complexes have provided more effective intracellular delivery of cytostatics or macromolecules which in the schemes are counting on cell membrane markers [14]. For a variety of specific organs and cells, the FA-promoted drug delivery can potentially minimize side effects while maximizing therapeutic efficacy. Thus, because of numerous FA advantages, researchers have been extensively developing this molecule as a cancer oriented agent [13].

The application of functionalized micelles in photodynamic therapy (PDT) could significantly increase the photosensitizer affinity to specific types of cancer cells. It is well known that the photodynamic procedure joins three intrinsically nontoxic factors, i.e. a photosensitizer (PS), light of proper wavelength, and oxygen, in the targeted tissue to produce cytotoxic reactive oxygen species (ROS), in particular singlet oxygen ($^1O_2$), to cause programmed cell death and necrosis. The ROS designation includes free radicals, e.g. atoms or molecules, which can exist independently and possess one or more unpaired electrons. For this group we can include also superoxide radical ($O_2^{\cdot}$–), hydroperoxyl radical ($HO_2^{\cdot}$), hydroxyl radical ($HO^{\cdot}$), peroxyl radical ($ROO^{\cdot}$), and alkoxyl radical ($RO^{\cdot}$), but also non-radicals, namely hydrogen peroxide (H_2O_2), singlet oxygen ($^1O_2$), and hypochlorous acid (HOCl). In typical cellular processes the reactive oxygen species, continuously generated in small amounts, may cause oxidative stress by means of oxidation of cellular membrane lipids, enzymes, tissue proteins, DNA, and carbohydrates, causing – at a certain point – irreversible cellular damage [15]. The fact that oxidative stress has been implicated in the etiology of several diseases and in aging is of major importance. On the other hand, it needs to be pointed out that the precise localization of the intentionally generated ROS is a crucial factor for achieving a therapeutic outcome. By allocated delivery of the photosensitizer, which may be accomplished by targeted drug delivery systems implementation, and light irradiation photodynamic treatment can minimize further damage to normal tissues in regards to other systemic modalities of the PDT treatment. Consequently, the photodynamic therapy has been established to treat cancer and other malignancies in recent years [16].

A very promising group of photosensitizers are metallophthalocyanines. This is because of their chemical stability, intense light absorption within the "therapeutic window" (600–800 nm), and extremely high ability to generate the singlet oxygen ($^1O_2$) [17]. Metallophthalocyanines, especially zinc (II) phthalocyanine and its derivatives, once illuminated with visible or infrared light, effectively generate highly ROS, which can bring about the cancer cells and tumor vasculature death [18]. Most of the recent research in this area deals with the development of chemical conjugation with peptides, ligands, antibodies, etc. or with the encapsulation of photosensitizers, comprising so-called third generation PDT agents that can be activated with a longer light wavelength, inducing stronger photosensitivity and, more importantly, providing enhanced tumor specificity [19].

Generally, zinc (II) phthalocyanine and its derivatives, both hydrophobic and hydrophilic/amphiphilic, show tendency to form dimers and aggregates, due to their planar structure and high aromaticity. Moreover the mentioned compounds may lose their photoactivity due to specific interactions with solvent molecules (hydrogen bonding to central ions or peripheral nitrogen atoms, electrostatic forces or π–π stacking). Numerous bulky peripheral groups (as tert-butyl or sulfonic acid) may suppress aggregation but still such microheterogenous solutions, of such modified phthalocyanines have limited stability and are susceptible to unwanted photoprocesses as photobleaching. Even synthesis of zinc (II) phthalocyanine derivatives with precisely controlled amphiphilicity is not sufficiently active to retard aggregation to a sufficient extent, especially in aqueous systems [20]. Moreover, zinc (II) phthalocyane possess unique possibility to occur in a stable and photoactive sandwich structure with all solvent coordination sites freely available, so called α-ZnPc form, e.g. when solubilized within PMs hydrophobic core [21]. The mentioned phenomena were carefully investigated in our previous paper [22]. Thus, zinc (II) phthalocyanine – one of the simplest, but very tricky metallophthalocyanie – was chosen as a photosensitizer for our studies.

The present contribution continues and develops our earlier studies on the fabrication of new drug delivery systems (DDS), such as nanocapsules, nanospheres, and polymeric micelles (PMs), which are well suited for the hydrophobic photosensitizers encapsulation, their photophysical and colloidal characterization, as well as biological evaluation [19,23–25]. The main aim of the present study was to enhance the targeted delivery and the photodynamic action of zinc (II) phthalocyanine (denoted as ZnPc) – a second-generation photosensitizer – in multidrug resistant ovarian (SKOV-3) and human metastatic malignant melanoma (Me45) cells by implementation of biodegradable and biocompatible folate-functionalized polymeric micelles. The present study involves the evaluation of ROS generation during PDT (Scheme 1), cellular internalization of nanocarriers, and cytoskeletal analysis of reorganization after PDT.

It should be emphasized here that currently studied polymeric micelles, one of the most promising group of nanocarriers, can be fabricated with methods showing low energy consumption as well as a potential for upstream optimization for large-scale production. PMs are known as very impressive targeted DDS and well-defined nanocarriers of precisely defined architecture since they comprise self-assembling structures that are easy-to-fabricate. Especially micelles of diblock copolymer methoxypoly(ethylene oxide)-b-poly(L-lactide) (mPEG-*b*-PLLA), functionalized with folic acid modified block copolymer (FA-PEG-b-PLLA), are characterized by highly active external surface and many interesting features, such as micellar pseudophases that provide a suitable solubilization for hydrophobic payloads [3,20]. The strongly

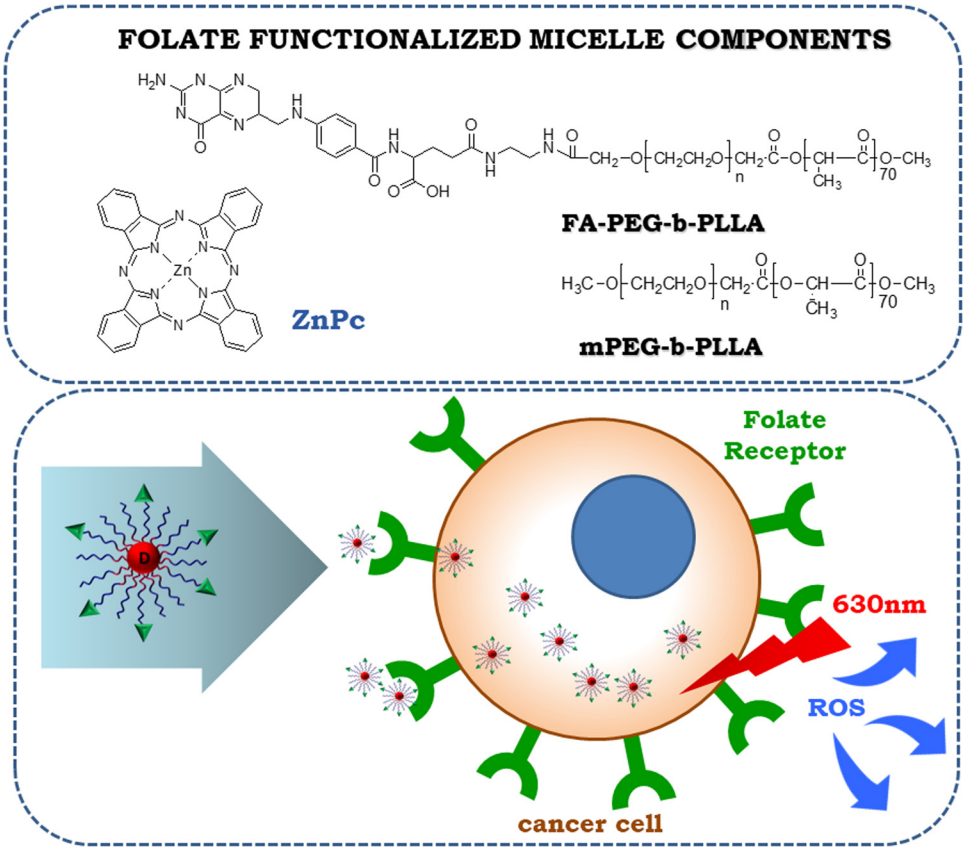

Scheme 1. The schematic representation of functionalized micelles composition and action.

hydrophobic ZnPc, solubilized in the studied FA-PEG-b-PLLA / mPEG-b-PLLA micelles, is protected against aggregation and deactivation, and possesses a significantly reduced vulnerability to photobleaching and an enhanced ability to generate ROS [23]. Additionally, FA-PEG-b-PLLA synthesis may be carried out in mild conditions by utilizing convenient, one-step reactions and simple purification techniques. Similarly, preparation of ZnPc-loaded folic acid modified polymeric micelles via dialysis method constitutes a simple and reproducible synthetic route. The studied FA-PEG-b-PLLA / mPEG-b-PLLA micelles with active payload provide both passive (EPR effect and prolonged systemic circulation due to "stealth" properties of PEG chains) and active (conjugation with ligand – folic acid) targeting [3].

2. Experimental

2.1. Chemicals

Block copolymer of methoxy poly(ethylene oxide), poly(L-lactide) (mPEG45-PLLA70, MW ≈ 7000), and folate – poly(ethylene glycol) – carboxylic acid (FA-PEG – COOH, MW ≈ 3000) were obtained from Akina, Inc. (West Lafayette, IN, USA). Zinc(II) phtalocyanine (ZnPc, 97%), poly(L-lactide) (PLLA, MW ≈ 5000), 9,10-anthracenediyl-bis (methylene)dimalonic acid sodium salt, trypsin-EDTA, Triton X-100 and DPX, as well as human serum albumin (HSA) were supplied from Sigma-Aldrich (St. Louis, MO, USA). TBA and DTNB (5,5′-dithiobis^{-2}-nitrobenzoic acid 3,3′-6) were obtained from Fluka (Germany). Trichloric acid (TCA), carboxy-H_2DCFDA, and dialysis bags (cut-off: 3.5 kDa) were purchased from Roth (Carl Roth, Germany). Fluorescence mounting medium for microscopic slides preparation was received from Dako (Denmark). All solvents applied in the present study were of analytical grade and were obtained from POCh (Gliwice, Poland). Water used for all experiments was doubly distilled.

2.2. Synthesis of folic acid modified poly(ethylene oxide) and poly(L-lactide) diblock copolymer

Folic acid functionalized block copolymer of poly(ethylene oxide) and poly(L-lactide) (FA-PEG-*b*-PLLA) was synthesized by esterification of pegylated folic acid with terminal carboxylic acid group (FA-PEG-COOH) and poly(L-lactide) (PLLA) in Steglich conditions [26,27]. FA-PEG-COOH (0.1 g, 0.0333 mmol), PLLA (0.1667 g, 0.0333 mmol), *N*,*N*-dicyclohexylcarboimide (DCC, 0.0076 g, 0.037 mmol), and *N*,*N*-dimethylpyridine (catalyst) in DMSO (10 mL) were stirred for 48 h. By-product (*N*,*N*-dicycloahexylurea) was filtered off and the desired product was obtained by dialysis (MWCO 8000, 72 h, 3 × 5 L of distilled water), followed by freeze drying (0.1665, 63% yield).

2.3. Structural identification and characterization of folic acid modified poly(ethylene oxide) and poly(L-lactide) diblock copolymer by FTIR and ^{1}H NMR spectroscopies

FTIR spectra of the obtained product as well as of the two major substrates (FA-PEG – COOH and PLLA) were recorded on a Fourier transform, Bruker VERTEX 70 V vacuum spectrometer (Rheinstetten, Germany). The measured samples were positioned on the diamond crystal of the ATR accessory. The results are shown in Fig. 1a. ^{1}H NMR spectra for FA-PEG-*b*-PLLA, FA-PEG – COOH, and PLLA were recorded on Bruker AMX600 instrument in DMSO-d_6, containing TMS as an internal reference. The obtained spectra were processed using TopSpin software and are shown in Fig. 1b.

2.4. Preparation of functionalized polymeric micelles – empty and with zinc (II) phthalocyanine

mPEG-b-PLLA / FA-PEG-b-PLLA micelles encapsulated with ZnPc were obtained using a modified dialysis method accordingly to Lv et al.

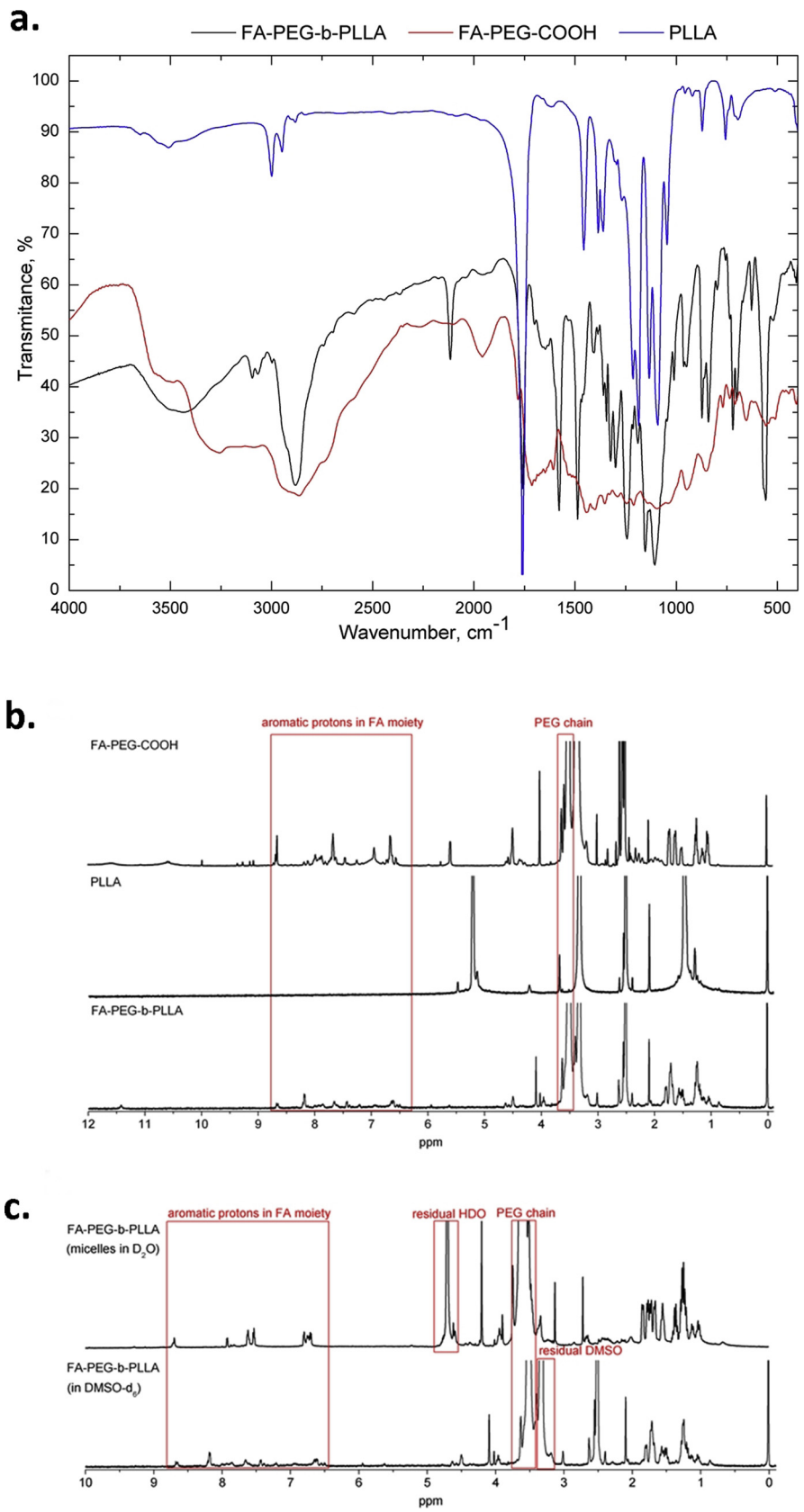

Fig. 1. The representation of FTIR spectra of FA-PEG-b-PLLA, folic acid functionalized poly(ethylene oxide) and poly(L-lactide) (a) and ^{1}H NMR spectra of FA-PEG-b-PLLA, folic acid functionalized poly(ethylene oxide) and poly(L-lactide) (b) as well as FA-PEG-b-PLLA in DMSO-d_6 and folate functionalized polymeric micelles in D_2O (c).

Table 1
Characteristics of the obtained ZnPc-loaded mPEG-b-PLLA / FA-PEG-b-PLLA micelles: cargo concentration, loading content, size and its distribution (denoted as polydispersity index, PdI).

System	Mole fraction of FA-PEG-*b*-PLLA	c_{ZnPc} [mg/ml]	c_{ZnPc} [μM]	LC [%]	PdI	D_H [nm]
T = 0						
1	0%	0.0172	29.7	0.86	0.285	126.9
2	1%	0.0138	24.0	0.69	0.188	67.31
3	5%	0.0265	45.8	1.33	0.268	61.91
4	10%	0.0213	36.9	1.06	0.264	56.54
5	100%	0.0172	29.7	0.86	0.154	68.18
T = 40 days						
1	0%	0.0170	29.7	0.86	0.288	127.9
2	1%	0.0140	24.1	0.69	0.187	68.87
3	5%	0.0260	45.6	1.32	0.279	63.85
4	10%	0.0210	36.8	1.06	0.266	57.09
5	100%	0.0170	29.6	0.86	0.150	67.68
T = 180 days						
1	0%	0.0172	29.7	0.86	0.280	123.4
2	1%	0.0135	23.9	0.69	0.188	66.83
3	5%	0.0271	46.0	1.34	0.258	62.94
4	10%	0.0213	36.9	1.06	0.269	59.11
5	100%	0.0177	29.9	0.86	0.164	64.33

[27]. With regards to the loaded PMs, zinc phthalocyanine was firstly dissolved in DMSO with a concentration of 0.2 mg/mL. Then, an appropriate volume of ZnPc stock solution in DMSO was added to 20 mg of block copolymers FA-PEG-b-PLLA and mPEG-b-PLLA mixture. Finally, the obtained mixtures were filtered and added dropwise to 10 mL of water. Organic co-solvent was removed from the mixtures by dialysis (MWCO 3500, 72 h, 3 × 5 L of distilled water).

2.5. Characterization of polymeric micelles

2.5.1. Dynamic light scattering (DLS)

The size and distribution magnitudes of the studied, freshly prepared polymeric micelles, and of those stored in the dark for 40 and 180 days, were estimated by DLS measurements at 25 °C by means of a Zetasizer Nano Series from Malvern Instruments with the 173° detection angle in optically homogeneous polystyrene cells. The DLS (Nano) program was utilized for the data evaluation. The acquired values of hydrodynamic diameter (D_H) and polydispersity index (PdI) are listed in Table 1, where PdI comprises a dimensionless degree of broadness of the particle size distribution [22].

2.5.2. Atomic Force Microscopy (AFM)

A Veeco NanoScope Dimension V AFM with an RT ESP Veeco tube scanner made possible the evaluation of the polymeric micelles' morphology. The scanning speed was 0.5 Hz, and a low-resonance-frequency pyramidal silicon cantilever resonating at 250–331 kHz was employed (at a constant force of 20–80 N/m). The amplitude of the resonance was set manually to the lowest possible value for stable imaging within the contamination layer present on the surface. The PMs were allowed to adsorb on a cover glass surface for 12 h by dipping them in the suspension before observation. Then the substrate surplus was rinsed from the surfaces by double distilled water for at least 1 min and the cover glass was dried at RT (room temperature) [23]. The obtained image as well as DLS graphs are shown in Fig. 2.

2.5.3. UV–vis spectroscopy in drug loading content determination

ZnPc content in mPEG-b-PLLA / FA-PEG-b-PLLA micelles was spectrophotometrically measured following the procedure in Lamch et al. [23]. Consequently, a sample of the PMs solution was diluted with an equal volume of water and then with five volumes of THF. Furthermore, the obtained solutions were measured using a U-2900 UV–vis spectrophotometer (Hitachi, Japan), and the maximal absorbance was detected at about 666 nm. To get the calibration curve, free ZnPc samples were prepared in 5:1 (v/v) THF:water mixture. The percent loading content (LC%) of ZnPc was estimated using the below given formula:

$$\%\text{loading content} = \frac{\text{weight of ZnPc in micelles}}{\text{weight of micelles}} 100\% \quad (1)$$

2.5.4. Proton nuclear magnetic resonance (^1H NMR)

Functionalized polymeric micelles, loaded with ZnPc, were evaluated by ^1H NMR to examine core-shell architecture, as well as to investigate the location of hydrophobic cargo in the polymeric micelles core and of folic acid within their corona. NMR spectra were recorded on a Bruker AMX600 instrument in deuterated DMSO (for block copolymer FA-PEG-*b*-PLLA) and D_2O (for folic acid functionalized polymeric micelles). Before ^1H NMR measurements, functionalized polymeric micelles (loaded with ZnPc), prepared according to the procedures described in Section 1.4, were freeze dried from aqueous systems and dispersed in D_2O. The obtained ^1H NMR spectra for FA-PEG-*b*-PLLA block copolymer (dissolved in DMSO-d_6) and functionalized polymeric micelles (in D_2O), processed using TopSpin software, are shown in Fig. 1c.

2.5.5. Photoreactivity measurements in microheterogeneous systems

Photokinetic studies of photobleaching and $^1O_2$ generation in microheterogeneous systems were performed in open 1 cm optical path quartz cuvettes with continuous stirring using an OPTEL Fibre Illuminator (Opole, Poland) with a long-pass glass filter (SCHOTT GLASWERKE GmbH, Mainz, Germany) to separate the 600–750 nm spectral interval. The photobleaching rate was evaluated spectrophotometrically by monitoring the ZnPc absorption spectrum in the range of 300–800 nm upon exposure to the lamp working at a 100 mW/cm^2 fluence 3 mL of solutions containing free or encapsulated ZnPc form in FA-functionalized PMs (System 4 in Table 1). Measurements for free ZnPc were conducted in 1% poly(ethylene glycol) water solution to prevent aggregation and loss of absorbance. In the photobleaching measurements the solution concentrations were selected in order to obtain an initial ZnPc main Q-band peak (669 nm) absorbance of less than 1.0. For both free and encapsulated ZnPc the measurements were performed at approximately 10 different irradiation time intervals. The rate of $^1O_2$ generation was measured in the same manner as photobleaching, that is in the presence of 0.14 mM 9,10-anthracenediyl-bis (methylene)dimalonic acid sodium salt (ABMDMA) [28,29]. The concentration of ZnPc was 5 μM in both the free and PM-encapsulated forms. The singlet oxygen generation rate constant (k_v) was calculated from the ratio of ABMDMA absorbance at 400 nm before and after irradiation as a function of the irradiation time according to Lamch et al. [22]. The photobleaching and $^1O_2$ generation measurements results are represented in Fig. 2c.

2.6. Cell lines and cultivation

In the current study, Me45 (human malignant melanoma), HaCaT (immortalized human keratinocytes from histologically normal skin), and SKOV-3 (cisplatin-resistant human ovarian cell line) were used. Me45 cells were a kind gift from Maria Sklodowska-Curie Memorial Cancer Center and Institute of Oncology Gliwice Branch, while SKOV-3 cells were a kind gift from Professor *J*. Golab from the Department of Immunology, Center of Biostructure Research and Medical University of Warsaw. HaCaT keratinocytes were purchased from the CLS Cell Lines Service GmbH (Germany). Me45 and HaCaT cell lines were grown in DMEM (Sigma, Poland) medium, while SKOV-3 cells in McCoy's medium (IITD, Poland) including 10% of fetal bovine serum (FBS, Biowhittaker, Poland) and 1% of antibiotics (Penicillin/streptomycin, Sigma). For the experiments, the Me45, HaCaT, and SKOV-3 cells were

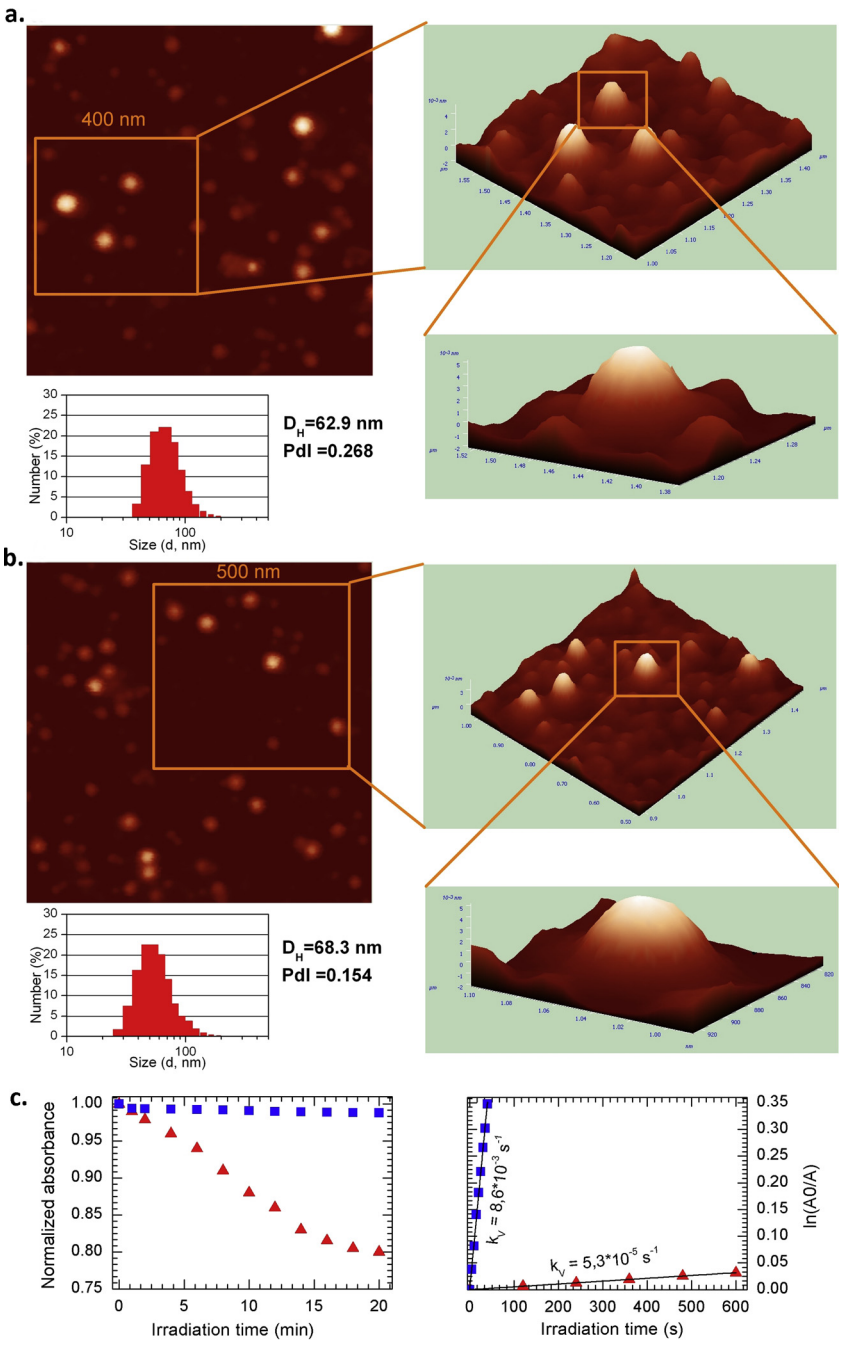

Fig. 2. Nanosystem characterization by AFM images and DLS spectra of functionalized polymeric micelles, loaded with zinc (II) phthalocyanine (for (a) system 1 and (b) system 4 as described in Table 1; and (c) by photobleaching (left) of FA-PEG-b-PLLA / mPEG-b-PLLA micelle-encapsulated (■) and free (▲) ZnPc in aqueous solution during irradiation with near-infrared light (100 mW/cm^2), as measured by UV–vis absorption spectra. Photooxidation (right) of 9,10-anthracenediyl-bis(methylene)dimalonic acid sodium salt upon irradiation in the presence of ZnPc: free (▲) and loaded in FA-PEG-b-PLLA / mPEG-b-PLLA micelles (■). k_v is the first-order rate constant for the photo-process as deduced from the slope of a semilog plot (denoted as natural logarithm of initial to final, for given period of time, absorbance values).

trypsinized (trypsin 0.025% and EDTA 0.02% solution; Sigma), rinsed twice with PBS, and maintained in a humidified atmosphere at 37 °C and 5% CO_2.

2.7. Cell viability (MTT) assay

The determination of cell viability after their exposition to the studied nanosystems was performed using the MTT cell proliferation assay (Sigma). The experimental protocol and conditions were set according to the procedure used during our prior research [30]. For the evaluation of cytotoxic impact, all the cell types were seeded onto 96-well plates (Nunc, Biokom, Poland) at a density of 2×10^4 cells in the final volume 200 µL of medium/well, and afterwards were incubated at 37 °C in 5% CO_2 atmosphere. Cells viability was determined after 24 h and 48 h for standard cytotoxicity *(dark cytotoxicity)* and after 24 h for photocytotoxicity, with various concentration of free and encapsulated ZnPc (1, 2, 3, and 4 µM). The details of the experimental conditions were described in our previous papers [19,23]. The absorbance from three duplicate experiments was measured at the wavelength of 570 nm using microplate reader (EnSpire, Perkin Elmer, Poland). The cell viability measured for each group was expressed as a percentage of control untreated cells. All experiments were performed in triplicate.

2.8. Photodynamic reaction

The cells were exposed to 4 µM concentration of zinc (II) phthalocyanine: free and encapsulated in the mPEG-*b*-PLLA / FA-PEG-*b*-PLLA micelles in complete media for 24 h in the dark. In the next stage, the cell culture medium was removed and replaced by fresh one, and cells were irradiated by the following light dose: 3 or 6 J/cm^2 utilizing a lamp (OPTEL, Opole, Fibre Illuminator, Poland) with polarized light (fluence rate at the level of the cell monolayer: 10 mW/cm^2) and a red

filter (λ_{max} = 632.8 nm). All measurements were realized at room temperature in semi-dark conditions. After irradiation, the cells were incubated at 37 °C and 5% CO_2 for 24 h in a humidified atmosphere [31].

2.9. Intracellular ROS quantification

For the ROS production cells were trypsynized and seeded on black 96-well plates with flat transparent bottom (Perkin Elmer, Poland) in concentration 2×10^4 per each well. After 24 h first photodynamic procedure (*2.8*) using two light does (3 and 6 J/cm^2), and then after 10 min DCF protocol was performed. Reactive oxygen production after photodynamic reaction (PDR) was determined using DCF (2,7-dichlorofluorescein) assay (Life Technologies, Poland). This DCF assay is based on the application of fluorescent properties of 6-carboxy-2,7-dichlorodihydrofluorescein diacetate 2,7-dichlorofluorescein (carboxy-H_2DCFDA). For experimentations, the concentrated stock solution of carboxy-H_2DCFDA (50 μg/mL in sterile DMSO) was kept at RT in the dark conditions and was subsequently properly diluted, following the manufacturer protocol, in cell culture medium without FBS. Then, the incubation medium was washed out from the cells with PBS containing 6 mM glucose, and the DCF reagent was added to the cell culture to achieve a final concentration of 10 μM and was left in darkness for 30 min long incubation at 37 °C. After this time the fluorescence was measured, where the excitation wavelength of 495 nm and emission wavelength of 530 nm were used. ROS level was detected by a multi-well scanning spectrophotometer (EnSpire Perkin Elmer, Poland).

2.10. F-actin staining and imaging- confocal laser scanning microscopy (CSLM) study

The confocal laser scanning microscopy (CLMS) was applied to determine the morphological changes of treated cells. SKOV-3 and Me45 cells were prepared for immunofluorescent reaction. The cells were seeded and grown on coverslips. After 24 h free ZnPc or loaded in the mPEG-*b*-PLLA / FA-PEG-*b*-PLLA micelles in 4 μM concentration was added. Cells were incubated next 24 h, then culture medium was changed before irradiation (6 J/cm^2). Then cells after 24 h post PDT treatment were fixed with 4% paraformaldehyde (PFA, Roth) in PBS, permeabilized with 0.5% Triton X-100 (Sigma, Poland) in PBS (v/v) for 5 min, and blocked with 1% fetal bovine serum (FBS) in PBS (for 30 min at RT). The cells were gently rinsed in fresh PBS at every step of the procedure. The following antibodies were used: primary antibody monoclonal mouse F-actin antibody (2 μg/ml; Sigma-Aldrich) and secondary antibody AlexaFluor®488 conjugated (for 60 min at RT; 1:50; Sigma-Aldrich). For imaging, an Olympus FluoView FV1000 confocal laser scanning microscope (Olympus, Poland) was used. The images were documented by employing a Plan-Apochromat 60x oil-immersion objective.

2.11. Statistics

All the experiments where MTT assay or ROS evaluation were applied were statistically assessed. The differences in significance between the mean values of diverse cell groups, for $n \geq 3$, were assessed individually for each experiment with the t-test. In the statistical evaluations, $p \leq 0.05$ was treated as statistically significant for every data set. Statistical analyses were performed using the GraphPad Prism 7 software.

3. Results and discussion

3.1. Folic acid modified poly(ethylene oxide) and poly(L-lactide) diblock copolymer synthesis and structure analysis

The FA-directed micelles of block copolymers FA-PEG-*b*-PLLA and mPEG-*b*-PLLA were designed and fabricated for receptor-promoted delivery of zinc (II) phthalocyanine. FTIR was used to characterize FA-PEG-*b*-PLLA in comparison with pure PLLA and FA-PEG−COOH, as displayed in Fig. 1. For FA-PEG−COOH and FA-PEG-*b*-PLLA the peaks in the 2900–3600 cm^{-1} region, at about 3375 cm^{-1} and 2888 cm^{-1}, are assigned to the stretching vibrations of N−H (in the pterin ring) and C–H moieties. In the IR spectrum of FA-PEG-*b*-PLLA the distinctive sharp peaks at 1758 cm^{-1} and 1651 cm^{-1} are assigned to the stretching vibrations of the carbonyl (C═O) group in the PLLA block and amide moiety of FA-PEG-*b*-PLLA, respectively. The peaks corresponding to the twisting and bending vibrations of C−O−C in PEG chains (for FA-PEG−COOH and FA-PEG-*b*-PLLA) appeared at about 1110 cm^{-1} and 529 cm^{-1}, respectively. Characteristic vibration peaks at about 1188 cm^{-1}, attributed to C−O−C bonds in PLLA chains, were present in spectra of PLLA and FA-PEG-b-PLLA. A similar analysis (spectrum measurement of product - FA-PEG-*b*-PLLA and main substrates: PLLA and FA-PEG−COOH in good solvents for all chemicals - DMSO-d_6) was conducted by means of ^{1}H NMR spectroscopy. The ^{1}H NMR spectrum of FA-PEG-*b*-PLLA (Fig. 1b) reveals the respective peaks of folate moiety (weak signals at 7.1 ppm, 8.1 ppm, and ca. 1 ppm) as well as intensive signals connected with PEG chain (methylene protons in $-OCH_2CH_2-$ fragment at 3.6 ppm) and PLLA block (protons of methyl and methine groups at 1.6 ppm and 5.2 ppm, respectively). For comparison, ^{1}H NMR spectra of the two main substrates revealed similar signals in the aromatic region and at about 3.6 ppm (for FA-PEG−COOH) as well as at 1.6 ppm and 5.2 ppm for poly(L-lactide). The whole spectral analysis showed that the obtained product – folic acid modified poly(ethylene oxide) and poly(L-lactide) diblock copolymer – possesses both hydrophobic (poly(L-lactide) and hydrophilic (poly(ethylene glycol)) characteristics with the FA moiety chemically attached to the latter one.

3.2. Preparation and characterization of functionalized polymeric micelles of FA-PEG-b-PLLA

Functionalized polymeric micelles provide a very outstanding targeted DDS because of their required size, their diameter ranging between 10 and 150 nm [19,32], biocompatible property, easy-to-fabricate feature, and custom-designed nature of their self-assembling structures. The dimensions of polymeric micelles are suitable and enable avoiding the clearance by the first pass renal filtration as well as the recognition by the phagocytic system, and consequently they may achieve a longer time of circulation in the bloodstream [33,34]. The folic acid functionalized polymeric micelles, containing different amounts of FA-PEG-*b*-PLLA varying from 0 to 100% and loaded with zinc (II) phthalocyanine as the photosensitizer, were prepared via the dialysis method. This method is good for fabrication of polymeric micelles with payloads entrapped in the hydrophobic core, when both cargo and block copolymer are easily soluble in non-volatile organic solvents, e.g. DMSO.

The average size of the studied ZnPc-loaded FA-PEG-*b*-PLLA / mPEG-*b*-PLLA micelles (derived from DLS by means of hydrodynamic diameter, D_H) was between 57 nm (system 1 – empty polymeric micelles) and 127 nm (system 4) (see Table 1) and was in accordance with what was previously reported for mPEG-*b*-PLLA micellar aggregates [35], as well as for similar folic acid functionalized PEG-*b*-PLA polymeric micelles [36]. At this size range (less than 200 nm), PMs can freely leak from the mononuclear phagocytic system (MPS), thanks to which they acquire increased circulation time in blood. Tumor capillaries have pore cutoff size oscillating between 200 nm and 1.2 μm [37], and the polymeric micelles prepared in this study can easily extravasate into the tumor tissue. Moreover, the investigated nanocarriers in our group so far have had a narrow size distribution (PdI < 0.3), which could make them potentially suitable for the cancer protocol [3].

The proper morphology of nanocarriers is decisive for the development of DDSs in targeted anticancer therapeutic attempts. The AFM 3D image of the functionalized polymeric micelles loaded by

hydrophobic zinc (II) phthalocyanine presented in Fig. 2 a, b reveals on its semi-smooth surface certain roughness, although 2D images show somewhat smoother surface morphology. The images also lead to the conclusion that the nanocarriers are semi-spherical in shape, with sizes in the range of 50–120 nm, and prove that there was no tendency to aggregate among the nanosystems. Moreover, the composition of the polymeric micelles (e.g. fraction of folic acid functionalized block copolymer) as well as the cargo concentration did not tend to change the morphology of the obtained systems. Consequently, AFM studies proved that the sizes of the polymeric micelles were compatible with the hydrodynamic diameters predicted from DLS (size distribution spectra are also presented in Fig. 2 a, b).

Loading content (LC) of the PMs is generally affected by the affinity of a given drug to the micellar core, the hydrophobic core volume, and the solubility of the bioactive component [38]. The values of LC% for ZnPc encapsulated in FA-PEG-*b*-PLLA/mPEG-*b*-PLLA micelles are between about 0.69 and 1.33% (w/w). Moreover, it was observed (Table 1), that storing the polymeric nanocarriers under dark conditions during 6 months resulted in no signs of PMs aggregation phenomena. Therefore, the obtained PMs can be assumed as DDS of high stability. Stability of polymeric micelles systems was also confirmed by AFM and DLS analysis.

Studies of FA-PEG-*b*-PLLA block copolymer in DMSO-d_6 (which is an appropriate solvent for hydrophilic and hydrophobic parts) and of folate functionalized polymeric micelles, loaded with zinc (II) phthalocyanine, in D_2O demonstrated evidences of micelles formation (Fig. 1c). The obtained copolymer structure was acquired from the ^{1}H NMR spectroscopy and is described in Section 2.3. The ^{1}H NMR spectrum of FA-PEG-*b*-PLLA in DMSO-d_6 (Fig. 1c) shows full structural resolution of the whole molecule (visible are signals contributed by both the hydrophobic and hydrophilic parts as well as the folate moiety). On the other hand, in D_2O, only the signals assigned to $-OCH_2CH_2-$ fragments, as well as protons of folate group, were seen. The signals contributed by methyl and methine groups of hydrophobic blocks were not found in the spectrum [39]. The NMR spectrum analysis leads to a conclusion that the PLLA grouping creates a central, solid-like hydrophobic core that is able to diminish all possible interactions with the solvent molecules. According to our previous studies on cargo locus of zinc (II) phthalocyanine, this particular photosensitizer was located within the poly(ethylene oxide) and poly(L-lactide) diblock copolymer micelles core [22]. This fact was crucial for excellent photostability and the ability to generate cytotoxic singlet oxygen of ZnPc in polymeric micelles. Additionally, aromatic protons of hydrophobic zinc (II) phthalocyanine payload were also not present in spectrum in D_2O, indicating its locus within the polymeric micelles core [40]. The PEG blocks, as well as the folate moiety, interact to a required extent with the water molecules by means of the H-bonds formation to form an exterior hydrophilic corona extending into the bulk solution and stabilizing the polymeric micelle structure. The ^{1}H NMR studies confirmed that ZnPc is dispersed within the polymeric micelles core and does not interact with water molecules, while folate is responsible for the functionalized polymeric micelles' interactions with biological structures in the exterior hydrophilic corona.

3.3. Photostability and $^1O_2$ generation of ZnPc in nano-self assembling FA-PEG-b-PLLA

Photostability (i.e. resistance to photobleaching) and the ability of a photosensitizer to generate reactive oxygen species are fundamental for a photodynamic reaction [39,40]. Generally, the metallophthalocyanine-type photosensitizers are effective in the formation of very toxic, short-lived oxygen species after irradiation. The presence of these high levels of ROS in exposed cells may involve degeneration and disintegration of biological structures. Additionally, $^1O_2$, the main toxic species produced by phthalocyanines, can diffuse from a variety of nanocarriers (e.g. polymeric or hybrid nanoparticles and micellar aggregates) and initiate cytotoxicity in cancer cells [19,25]. Numerous organic dyes, including phthalocyanine-class photosensitizers, are vulnerable to photodegradation involving the loss of absorbance, fluorescence, and photoactivity, and for that reason the encapsulation methodology can appreciably eliminate these disadvantages [25,41–43].

Photochemical properties of ZnPc (photobleaching and $^1O_2$ generation rates) were measured in its free form and loaded in FA-PEG-*b*-PLLA/mPEG-*b*-PLLA micelles. The photobleaching process was presented by plotting the change in absorbance as a function of irradiation time (Fig. 2c, left panel). The achieved data clearly proved that the ZnPc encapsulated in the polymeric micelles showed better photostability during irradiation in regards to the native form of photosensitizer, which is in very good agreement with observations of ZnPc-loaded mPEG-b-PLLA micelles presented in our previous studies [22]. Similarly reduced photobleaching rates for the encapsulated form of photosensitizer were observed for other photosensitizers, such as ZnPc, Photofrin, and cyanine IR-780, or for SiPc loaded in various nanocarriers: PMs, polymeric or silica nanoparticles, and oil-core nanocapsules.

The first-order rate constants of $^1O_2$ generation were determined in the present contribution by means of photobleaching of ABMDMA under irradiation of free and encapsulated ZnPc in the presence of oxygen (see Fig. 2c, right panel). This indirect method was used since the $^1O_2$ phosphorescence, which is another indicator of the presence of the singlet oxygen, is hard to observe in water solutions [25]. The obtained results demonstrate that the chemical probe (9,10-anthracenediyl-bis(methylene)dimalonic acid sodium salt) was much more efficaciously (two orders of magnitude better; $k_v = 8.6 \times 10^{-5}$ s^{-1} in comparison to $k_v = 5.3 \times 10^{-5}$ s^{-1}, respectively) oxidized by the encapsulated in FA-PEG-*b*-PLLA/mPEG-*b*-PLLA micelles ZnPc than by its free form. A very similar phenomenon was observed for ZnPc encapsulated in mPEG-*b*-PLLA micelles [22] prepared in a slightly different manner. The calculated values of k_v constants for ZnPc-loaded mPEG-b-PLLA and FA-PEG-*b*-PLLA/mPEG-*b*-PLLA micelles (8.8×10^{-5} s^{-1} and 8.6×10^{-5} s^{-1}, respectively) clearly indicate that the presence of folic acid in the polymeric micelles corona has no effect on the generation of $^1O_2$ by encapsulated phthalocyanine.

Thus, the obtained photobleaching and $^1O_2$ generation data remain satisfactorily in line with our other studies [25], and the excellent photochemical properties of ZnPc-loaded FA-PEG-*b*-PLLA/mPEG-*b*-PLLA micelles may be ascribed to the active compound located within the hydrophobic micellar core. The photobleaching studies are congruent with the $^1O_2$ generation results: encapsulation of ZnPc postpones photobleaching and enhances ROS production. Both of these features are strictly related to the appropriate properties of polymeric micelles core microenvironment.

3.4. Intracellular uptake of encapsulated ZnPc

The assessment of the intracellular distribution of ZnPc loaded in nanocarriers determines the efficacy of future clinical or biological applications. To find out whether zinc (II) phthalocyanine loaded into folate functionalized polymeric micelles can get at the intracellular compartment, the emission of ZnPc red fluorescence was analyzed by confocal scanning laser microscopy (CLSM). CSLM images of ZnPc (free or encapsulated in the functionalized polymeric micelles) internalized by Me45 and SKOV-3 cells are shown in Fig. 3 (the upper panel of the microphotographs). The intracellular distribution indicates that ZnPc was more efficiently delivered in the micelles functionalized with folic acid (samples Nos 2–5 in melanoma cells and samples Nos 2, 3, and 5 in ovarian cancer cells). Phthalocyanine was distributed mainly in cytoplasm. However, in ovarian cancer cells, ZnPc delivered in micelles with folic acid condensed nearby the nuclear envelope. Close-nuclei localization of the used photosensitizer may be significant in future targeted therapeutic procedures.

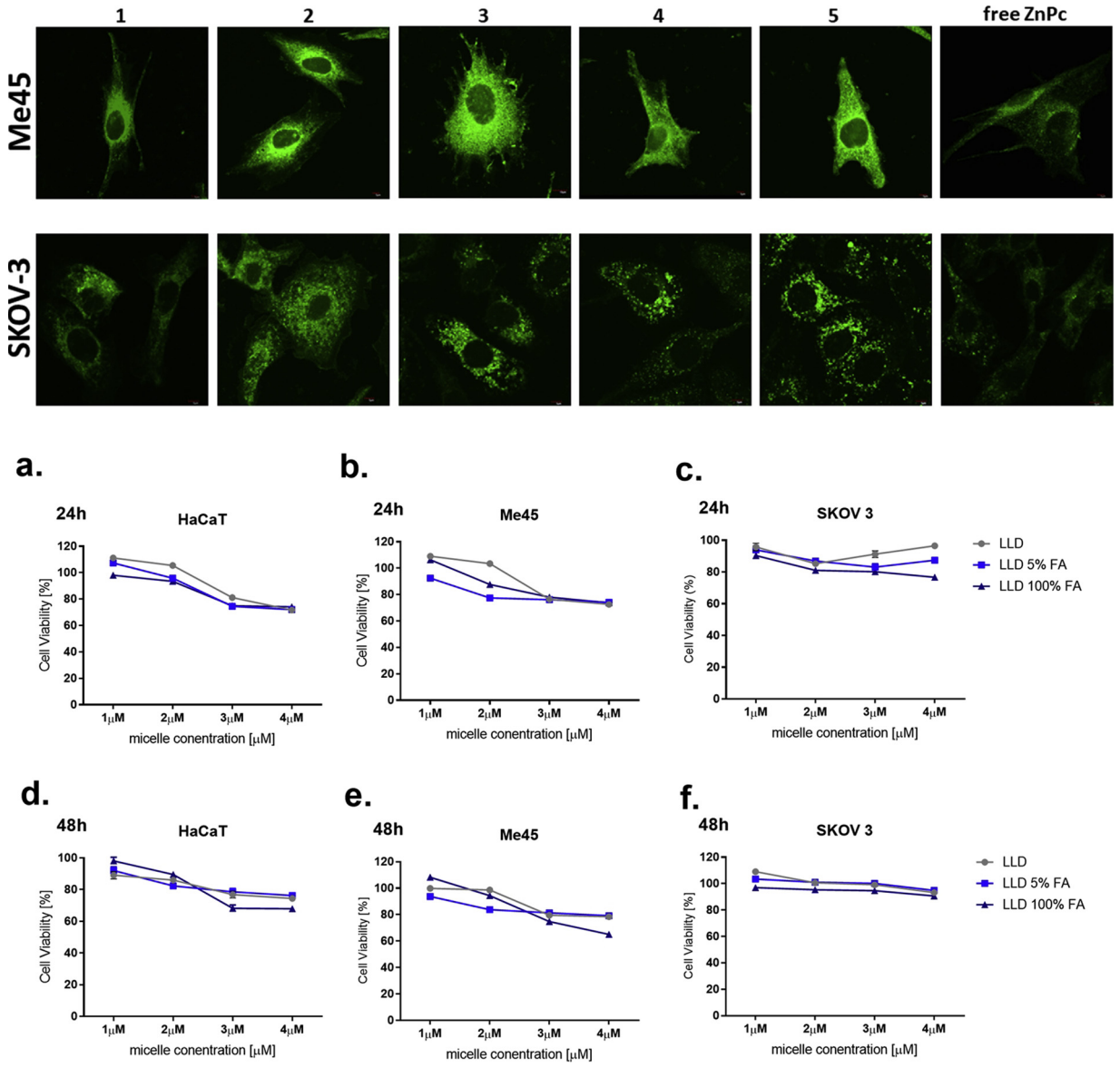

Fig. 3. The biological micelles evaluation by internalization of folic acid (FA) functionalized polymeric micelles by cancer cell lines visualized by CLSM study; metastatic melanoma (Me45) – upper panel; resistant ovarian cells (SKOV-3) – bottom panel; nanosystems were used as follows: 1-0% FA; 2 – 1% FA; 3–5% FA; 4–10% FA; 5–100% FA). The cytotoxicity determination of empty folic acid functionalized polymeric micelles and polymeric micelles without folic acid after 24 h of incubation in (a) HaCaT; (b) Me45; (c) SKOV-3 cells or 48 h of incubation in (d) HaCaT; (e) Me45; (f) SKOV-3 cells. *SD for* $n \geq 3$.

3.5. Cyto- and photocytotoxicity studies

The effectiveness of PDT and the phototoxic effect strongly depend on the photosensitizer's transport's efficacy through cancer cells' membranes to perform its anticancer action. The most important part of the therapeutic forecasting is the targeted drug delivery. Our research shows that the photosensitizer encapsulated in PMs "decorated with "folic acid can be more effective in comparison to the photosensitizer free from folic acid. The application of the targeted nanoproducts can also increase the phototoxic effect in malignant tissues. The cyto- and photocytotoxicity measurements were made on human metastatic melanoma and normal keratinocytes, as well as on cisplatin-resistant human ovarian cell line. Diagrams showing cytotoxicity of empty micelles in Me45, SKOV-3, and HaCaT cells are presented in Fig. 3 a–f. A low cytotoxic impact of empty nanocarriers was observed in all the tested cell lines even after long time of incubation (48 h). The results of cytotoxic influence of free and encapsulated ZnPc in polymeric micelles are shown in Fig. 4 a–f. The results after 24 h incubation reveal statistically significant cytotoxic effect in normal keratinocytes (Fig. 4a). However, after 48 h we could observe cell recovery measured as an increased oxidoreductive signal (Fig. 4d). In case of cancer cells, a slight decrease of cell viability was observed, in particular in SKOV-3 cells. This may indicate that the cells with folate receptor overexpression take up more ZnPc. Photocytotoxic effectiveness of both free and encapsulated in polymeric micelles ZnPc in Me45 and SKOV-3 is shown in Fig. 5a and b. The "dark cytotoxicity" studies indicated that ZnPc incorporated in micelles was not lethal for cells. In particular, this was the case after longer time of exposition (48 h) to nanosystems in normal and cancer cells. Our previous studies with ZnPc in polymeric micelles also indicated low "dark toxicity" in cancer and normal cells (keratinocytes and epithelial cells) [20]. Photodynamic reaction performed in both cell lines displayed increasing photocytotoxicity with the increasing percentage of folic acid functionalization and increasing irradiation dose (Fig. 5a and b). Similar studies were performed by Luong et al. on cells overexpressing folate-receptor (ovarian-SKOV-3 and cervical cancer-HeLa cells). Cells were treated with PMs loaded

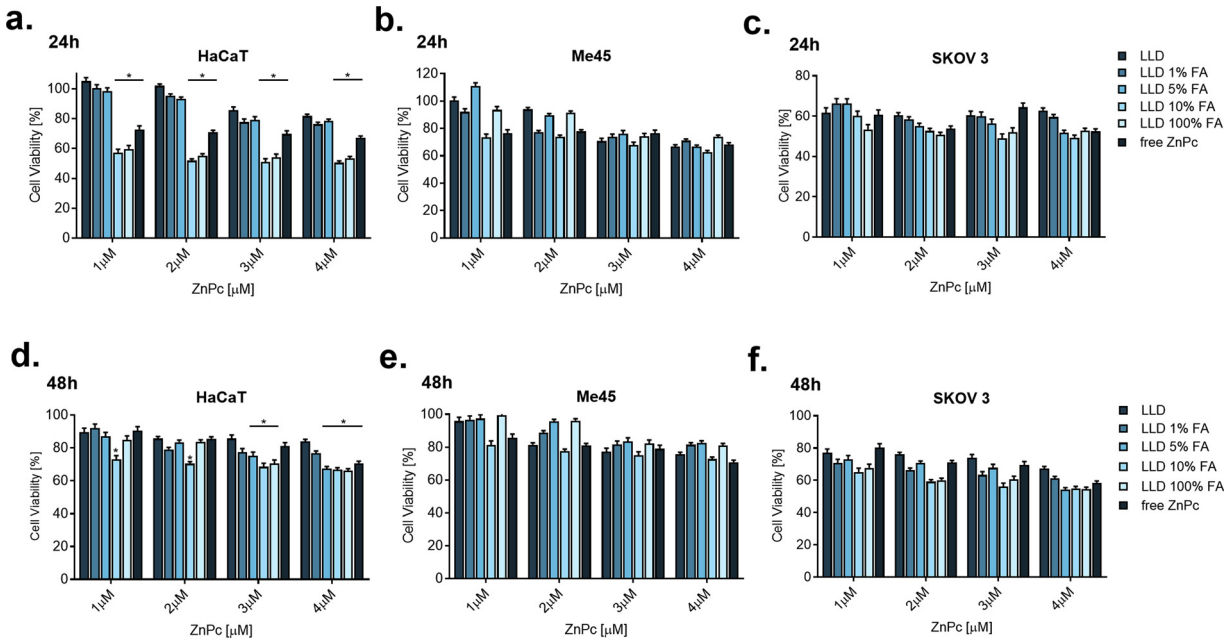

Fig. 4. Cytotoxicity of zinc (II) phthalocyanine encapsulated in folic acid functionalized polymeric micelles and polymeric micelles without folic acid as well as free ZnPc after 24 h of incubation in (a) HaCaT; (b) Me45; (c) SKOV-3 cells or 48 h of incubation in (d) HaCaT; (e) Me45; (f) SKOV-3 cells. SD for $n \geq 3$; $^{*}p \leq 0.05$.

with synthetic curcumin-difluorinated (CDF) analog and functionalized by FA. Cells exhibited high anticancer activity and underwent apoptotic cell death [44]. Zhou et al. used FA-functionalized polymeric micelles (PCL-b-PEO-FA) for intravesical instilled chemotherapy and also proved that cells with FA receptors (T-24 cell) were more powerful in terms of drug delivery than normal cells (HEK-293) [45].

3.6. Reactive oxygen species (ROS) generation in the cancer cells

In the next stage, reactive oxygen species release was determined as one of the crucial factors indicating PDT efficacy. ROS generated during PDT reactions have been proven to damage effectively cancer cells by multifactorial mechanisms. The effect of oxidative stress activation is mostly triggered by the ROS-mediated oxidation of DNA, polyunsaturated fatty acids in lipids, and amino acids in proteins. Moreover, antioxidant responses can be included in the direct effects of oxidation, such as the activation of mitogen-activated protein kinase (MAPK) cascades, the extracellular signal-related kinases (ERK), the c-Jun N-terminal kinases (JNK), and p38 MAPK, which determine cellular responses through downstream signaling pathways [46]. Furthermore, ROS can also contribute to the closure of blood vessels, as the result of which cancer cells have limited access to oxygen and nutrients.

The level of ROS in Me45 and SKOV-3 cells is presented in Fig. 5c and d. Reactive oxygen species increase was significantly stimulated after irradiation in both cancer cell lines. However, melanoma cells responded more intensively after a stronger dose of irradiation (6 J/cm^2). The augmented release of ROS led to a significant photodynamic effect and induced programmed cell death in the treated cancer cells.

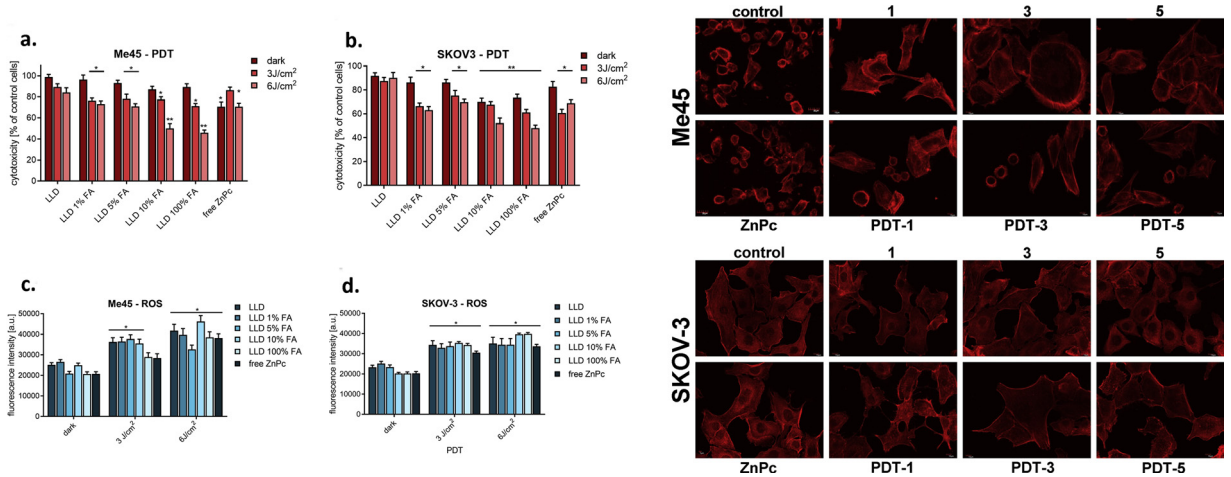

Fig. 5. The photodynamic efficacy determined by cellular viability after incubation with 4 μM concentration of free ZnPc and ZnPc-loaded mPEG-*b*-PLLA/FA-PEG-*b*-PLLA micelles at varying folic acid concentration and photodynamic reaction performed utilizing irradiation dose of 3 and 6 J/cm^2 in (a) Me45 and (b) SKOV-3 cells. The level of ROS in (c) Me45 and (d) SKOV-3 cells after photodynamic reaction with polymeric micelles. Cells were treated with 4 μM concentration of free and encapsulated ZnPc. SD for $n \geq 3$; $^{*}p \leq 0.05$.
The right panel - The evaluation of cellular cytoskeleton protein (F-actin) in Me45 (upper microphotographs) and SKOV-3 (bottom) cells after photodynamic reaction with polymeric micelles. **PDT-1** – photodynamic therapy with micelles No.1 (0% FA); **PDT-3** – photodynamic therapy with micelles No.3 (5% FA); **PDT-5**– photodynamic therapy with micelles No.5 (100% FA). Cells were treated with 4 μM concentration of ZnPc: alone and encapsulated.

The experiments with ROS generation and singlet oxygen production (described in subsection 2.3) revealed that the ZnPc-loaded FA-PEG-*b*-PLLA/mPEG-*b*-PLLA micelles have the potential for developing PDT applications in comprehensive cancer treatment. In another research, ZnPc in polymeric micelles was also utilized for photodynamic therapy of osteosarcoma. Authors observed that PEG-PMAN/ZnPc nanoparticle (PPZ) intensely provoked reactive oxygen species generation after light irradiation and mitochondrial injury, and promoted arrest of cell cycle at G2/M [47].

3.7. Cytoskeleton reorganization after PDR

It has been shown that ROS have a significant impact upon the cytoskeletal dynamics and organization, and can activate regulated cell death [48]. The actin cytoskeleton plays an outstanding role in the apoptosis process, which implies shifts in actin filament organization at various steps of apoptosis. In our study, F-actin was evaluated after exposition to nanosystems and after photodynamic procedure with free ZnPc and ZnPc-loaded mPEG-b-PLLA/FA-PEG-b-PLLA micelles. The obtained results are presented in Fig. 5 (the right panel containing the microphotographs). Before irradiation we noticed the presence of circular formation of actin cytoskeleton in the case of Me45 cells. Photodynamic reaction induced structural changes in the spindle shaped F-actin cytoskeleton of Me45 cells. SKOV-3 cells exposed only to free ZnPc and ZnPc in nanosystems did not reveal any cytoskeleton reorganization. However, on PDT we observed low density of actin fibers inside of cells and near nuclei. This data reveals that PDT-mediated ZnPc-loaded mPEG-b-PLLA/FA-PEG-b-PLLA micelles induce morphological changes in cancer cells. Also, Juarranz et al. (2001) indicated that cytoskeletal constituents were found to cause cell damage and death by ZnPc photosensitization [49].

The analysis of the impact of photocytotoxicity, reactive oxygen species (ROS) generation, and cytoskeleton organization confirmed enhanced efficiency of encapsulated ZnPc in comparison to the free photosensitizer. Additionally, folate (FA) functionalized micelles may find a specific application, because folate receptors are known to be overexpressed on the surface of certain tumor cells in comparison to the healthy cells. Thus, functionalized nanocarriers are proposed here as a profound vehicle for active targeting-based therapies. Moreover, in comparison to protein ligands, FA is relatively easy to obtain chemically, more stable, of smaller size, and non-immunogenic [50].

4. Conclusions

Zinc (II) phthalocyanine loaded folate-functionalized polymeric micelles were fabricated by self-assembly of the synthesized block copolymer FA-PEG-*b*-PLLA and mPEG-*b*-PLLA. DLS methodology confirmed the polymeric micelles to be below 150 nm in diameter and to have low polydispersity index and good colloid stability of the studied nanocarriers, while AFM was used to investigate their morphology. Thus, the size optimization enables better prediction of the passive cellular uptake and in future in vivo applications may improve targeting through the EPR system. The ^{1}H NMR analysis revealed evidences that ZnPc is located within the polymeric micelles core, while folate, responsible for the interactions of the functionalized polymeric micelles with biological structures, is located in the exterior hydrophilic corona. The functionalized micelles developed in this study exhibited higher cytotoxicity toward cancer cells with overexpressed folate receptors than the unfunctionalized standard micelles. The internalization studies acknowledged that folate-grafted mPEG-b_PLLA nanocarriers provided the enhanced drug uptake within cancer cells that increased with the percentage of functionalization. The FA engineered polymeric micelles have numerous benefits, such as high ZnPc loading with the ability to deliver increased doses of ZnPc to cancer cells overexpressing FA-receptor. Moreover, numerous studies confirm micelles as biologically safe and biocompatible. Our results prove that the obtained functionalized polymeric micelles are promising nanocarriers for the PDT procedures, but further investigations are still required.

Disclosure of interest

The authors declare that they have no competing interests.

Acknowledgements

The work was supported by the Wrocław Research Center EIT + under the project 'Biotechnologies and advanced medical technologies'-BioMed (POIG 01.01.02-02-003/08-00) financed from the European Regional Development Fund Operational Programme Innovative Economy (1.1.2.) and by a statutory activity subsidy from the Polish Ministry of Science and Higher Education for the Faculty of Chemistry of Wrocław University of Technology. The authors are very grateful to Professor Stephen Beebe from Old Dominion University (Virginia, USA) for his valuable, constructive suggestions and the linguistic assistance with this manuscript.

References

[1] H. Chen, L. Xiao, Y. Anraku, P. Mi, X. Liu, H. Cabral, A. Inoue, T. Nomoto, A. Kishimura, N. Nishiyama, K. Kataoka, Polyion complex vesicles for photoinduced intracellular delivery of amphiphilic photosensitizer, J. Am. Chem. Soc. 136 (2014) 157–163.
[2] M. Chudy, K. Tokarska, E. Jastrzębska, M. Bułka, S. Drozdek, Ł. Lamch, K.A. Wilk, Z. Brzózka, Lab-on-a-chip systems for photodynamic therapy investigations, Biosens. Bioelectron. 101 (2018) 37–51.
[3] Ł Lamch, A. Pucek, J. Kulbacka, M. Chudy, E. Jastrzębska, K. Tokarska, M. Bułka, Z. Brzózka, K.A. Wilk, Recent progress in the engineering of multifunctional colloidal nanoparticles for enhanced photodynamic therapy and bioimaging, Adv. Colloid Interface Sci. 261 (2018) 62–81, https://doi.org/10.1016/j.cis.2018.09.002.
[4] Ł Lamch, M. Tsirigotis-Maniecka, J. Kulbacka, K.A. Wilk, Synthesis of new zinc (II) phthalocyanine conjugates with block copolymers for cancer therapy, Arkivoc 2 (2017) 433–445.
[5] M.S. Bakshi, Colloidal micelles of block copolymers as nanoreactors, templates for gold nanoparticles, and vehicles for biomedical applications, Adv. Colloid Interface Sci. 213 (2014) 1–20.
[6] K. Loomis, K. McNeeley, R.V. Bellamkonda, Nanoparticles with targeting, triggered release, and imaging functionality for cancer applications, Soft Matter 7 (2011) 839–856.
[7] W. Xia, P.S. Low, Folate-targeted therapies for Cancer, J. Med. Chem. 53 (2010) 6811–6824.
[8] J. Sudimack, R.J. Lee, Targeted drug delivery via the folate receptor, Adv. Drug Deliv. Rev. 41 (2000) 147–162.
[9] J. Nicolas, S. Mura, D. Brambilla, N. Mackiewicz, P. Couvreu, Design, functionalization strategies and biomedical applications of targeted biodegradable/biocompatible polymer-based nanocarriers for drug delivery, Chem. Soc. Rev. 42 (2013) 1147–1235.
[10] Z. Hami, M. Amini, M. Ghazi-Khansari, S.M. Rezayat, K. Gilani, Synthesis and in vitro evaluation of a pH-sensitive PLA–PEG–folate based polymeric micelle for controlled delivery of docetaxel, Colloids Surf. B Biointerfaces 116 (2014) 309–317.
[11] M. Tsirigotis-Maniecka, Ł Lamch, I. Chojnacka, R. Gancarz, K.A. Wilk, Microencapsulation of hesperidin in polyelectrolyte complex microbeads: physicochemical evaluation and release behavior, J. Food Eng. 214 (2017) 104–116.
[12] A. Cunningham, N.R. Ko, J.K. Oh, Synthesis and reduction-responsive disassembly of PLA-based mono-cleavable micelles, Colloids Surf. B Biointerfaces 122 (2014) 693–700.
[13] P. Yu, X.-M. Xia, M. Wu, C. Cui, Y. Zhang, L. Liu, B. Wu, C.-X. Wang, L.-J. Zhang, X. Zhou, R.-X. Zhuo, S.-W. Huang, Folic acid-conjugated iron oxide porous nanorods loaded with doxorubicin for targeted drug delivery, Colloids Surf. B Biointerfaces 120 (2014) 142–151.
[14] X. Liu, Y. Zhang, D. Ma, H. Tang, L. Tan, Q. Xie, S. Yao, Biocompatible multi-walled carbon nanotube-chitosan-folic acid nanoparticle hybrids as GFP gene delivery materials, Colloids Surf. B Biointerfaces 111 (2013) 224-223.
[15] A. Gomes, E. Fernandes, J.L.F.C. Lima, Fluorescence probes used for detection of reactive oxygen species, J. Biochem. Biophys. Methods 65 (2005) 45–80.
[16] K. Lu, C. He, W.A. Lin, Chlorin-based nanoscale metal – organic framework for photodynamic therapy of colon cancers, J. Am. Chem. Soc. 137 (2015) 7600–7603.
[17] L.W. Yang, S.C. Mei, L. Qin, L. Nan, W.D. Zhou, Y.Y. Yuan, C.W. Xing, Synthesis and photoactivity of pH-responsive amphiphilic block polymer photosensitizer bonded zinc phthalocyanine, Sci. China 55 (2012) 1108–1114.
[18] S. Luo, E. Zhang, Y. Su, T. Cheng, C. Shi, A review of NIR dyes in cancer targeting and imaging, Biomaterials 32 (2011) 7127–7138.
[19] Ł Lamch, U. Bazylińska, J. Kulbacka, J. Pietkiewicz, K. Bieżuńska-Kusiak, K.A. Wilk, Polymeric micelles for enhanced Photofrin II® delivery, cytotoxicity and pro-apoptotic activity in human breast and ovarian cancer cells, Photodiagn. Photodyn.

Ther. 11 (2014) 570–585.
[20] N.A. Kuznietsova, N.S. Gretsova, V.M. Derkacheva, O.L. Kaliya, E.A. Lukyanets, Sulfonated phthalocyanines: aggregation and singlet oxygen quantum yield in aqueous solutions, J. Porphyr. Phthalocyanines 7 (2003) 147–154.
[21] H.K. Moon, M. Son, J.E. Park, S.M. Yoon, S.H. Lee, H.C. Choi, Significant increase in the water dispersibility of zinc phthalocyanine nanowires and applications in cancer phototherapy, NPG Asia Mater. 4 (2012) 1–8.
[22] Ł Lamch, W. Tylus, M. Jewgiński, R. Latajka, K.A. Wilk, Location of varying hydrophobicity zinc(II) phthalocyanine-type photosensitizers in Methoxy Poly(ethylene oxide) and poly(l-lactide) block copolymer micelles using 1H NMR and XPS techniques, J. Phys. Chem. B 120 (2016) 12768–12780.
[23] Ł Lamch, J. Kulbacka, J. Pietkiewicz, J. Rossowska, M. Dubińska-Magiera, A. Choromańska, K.A. Wilk, Preparation and characterization of new zinc(II) phthalocyanine – containing poly(L-lactide)-b-poly(ethylene glycol) copolymer micelles for photodynamic therapy, J. Photochem. Photobiol. B: Biol. 160 (2016) 185–197.
[24] J. Kulbacka, P. Pucek, M. Kotulska, M. Dubińska-Magiera, J. Rossowska, M.-P. Rols, K.A. Wilk, Electroporation and lipid nanoparticles with cyanine IR-780 and flavonoids as efficient vectors to enhanced drug delivery in colon cancer, Bioelectrochemistry 110 (2016) o19–31.
[25] S. Drozdek, J. Szeremeta, Ł Lamch, M. Nyk, M. Samoc, K.A. Wilk, Two-photon induced fluorescence energy transfer in polymeric nanocapsules containing $CdSe_xS_{1-x}$/ZnS Core/Shell quantum dots and zinc (II) phthalocyanine, J. Phys. Chem. C 120 (2016) 15460–15470.
[26] B. Neises, W. Steglich, Simple method for the esterification of carboxylic acids, Angew. Chem. Int. Ed. 17 (1978) 522–524.
[27] Y. Lv, B. Yang, T. Jiang, Y.-M. Li, F. He, R.-X. Zhuo, Folate-conjugated amphiphilic block copolymers for targeted and efficient delivery of doxorubicin, Colloids Surf. A Physicochem. Eng. Asp. 115 (2014) 253–259.
[28] M. da Volta Soares, M.R. Oliveira, E.P. dos Santos, L. de Brito Gitirana, G.M. Barbosa, C.H. Quaresma, E. Ricci-Júnior, Nanostructured delivery system for zinc phthalocyanine: preparation, characterization, and phototoxicity study against human lung adenocarcinoma A549 cells, Int. J. Nanomed. 6 (2011) 227–238.
[29] B. Zhao, J.-J. Yin, P.J. Bilski, C.F. Chignell, J.E. Roberts, Y.-Y. He, Enhanced photodynamic efficacy towards melanoma cells by encapsulation of Pc4 in silica nanoparticles, Toxicol. Appl. Pharmacol. 241 (2009) 163–172.
[30] A. Pucek, N. Niezgoda, J. Kulbacka, C. Wawrzeńczyk, K.A. Wilk, Phosphatidylcholine with conjugated linoleic acid in fabrication of novel lipid nanocarriers, Colloids Surf. A: Physicochem. Eng. Asp. 532 (2017) 377–388.
[31] P. Pietkiewicz, K. Zielińska, J. Saczko, J. Kulbacka, M. Majkowski, K.A. Wilk, New approach to hydrophobic cyanine-type photosensitizer delivery using polymeric oil-cored nanocarriers: hemolytic activity, in vitro cytotoxicity and localization in cancer cells, Eur. J. Pharm. Sci. 39 (2010) 322–335.
[32] M.J. Ernsting, M. Murakami, A. Roy, S.D. Li, Factors controlling the pharmacokinetics, biodistribution and intratumoral penetration of nanoparticles, J. Control. Release 172 (2013) 782–794.
[33] R. Misra, S. Acharya, S.K. Sahoo, Cancer nanotechnology: application of nanotechnology in cancer therapy, Drug Discov. Today 15 (2010) 842–850.
[34] G.S. Kwon, Polymeric micelles for delivery of poorly water-soluble compounds, Crit. Rev. Ther. Drug Carrier Syst. 20 (2003) 357–603.
[35] G. Gaucher, M. Dufresne, H. Vinayak, P. Sant, N. Kang, D. Maysinger, J.C. Leroux, Block copolymer micelles: preparation, characterization and application in drug delivery, J. Control. Release 109 (2005) 169–188.
[36] Z. Hami, M. Amini, M. Ghazi-Khansari, S.M. Rezayat, K. Gilani, Doxorubicin-conjugated PLA-PEG-Folate based polymeric micelle for tumor-targeted delivery: synthesis and in vitro evaluation, DARU 22 (2014) 30–36.
[37] Y. Bae, W.D. Jang, N. Nishiyama, S. Fukushima, K. Kataoka, Multifunctional polymeric micelles with folate-mediated cancer cell targeting and pH triggered drug releasing properties for active intracellular drug delivery, Mol. Biol. Syst. 1 (2005) 242–250.
[38] Z.L. Tyrrell, Y. Shen, M. Radosz, Fabrication of micellar nanoparticles for drug delivery through the self-assembly of block copolymers, Prog. Polym. Sci. 35 (2010) 1128–1143.
[39] C.R. Heald, S. Stolnik, K.S. Kujawinski, C. De Matteis, M.C. Garnett, L. Illum, S.S. Davis, S.C. Purkiss, R.J. Barlow, P.R. Gellert, Poly(lactic acid)-poly(ethylene oxide) (PLA-PEG) nanoparticles: NMR studies of the central solid like PLA core and the liquid PEG corona, Langmuir 18 (2002) 3669–3675.
[40] E. Blanco, E.A. Bey, Y. Dong, B.D. Weinberg, D.M. Sutton, D.A. Boothman, J. Gao, B-lapachone-containing PEG-PLA polymer micelles as novel nanotherapeutics against NQO1-overexpressing tumor cells, J. Control. Release 122 (3) (2007) 365–374.
[41] L. Benov, Photodynamic therapy: current status and future directions, Med. Princ. Pract. 24 (s1) (2015) 14–28.
[42] M.C. DeRosa, R.J. Crutchley, Photosensitized singlet oxygen and its applications, Coord. Chem. Rev. 233-234 (2002) 351–371.
[43] M.C. García Vior, J. Marino, L. Roguin, A. Sosnik, J. Awruch, Photodynamic effects of zinc(II) phthalocyanine-loaded polymeric micelles in human nasopharynx KB carcinoma cells, Photochem. Photobiol. 89 (2013) 492–500.
[44] D. Luong, P. Kesharwani, H.O. Alsaab, S. Sau, S. Padhye, F.H. Sarkar, A.K. Iyer, Folic acid conjugated polymeric micelles loaded with a curcumin difluorinated analog for targeting cervical and ovarian cancers, Colloids Surf. B Biointerfaces 157 (2017) 490–502.
[45] D.H. Zhou, G. Zhang, Gan Z.H. Yu QS, Folic acid modified polymeric micelles for intravesical instilled chemotherapy, Chin. J. Polym. Sci. 36 (4) (2018) 479–487.
[46] W.J. Shen, C.Y. Hsieh, C.L. Chen, K.C. Yang, C.T. Ma, P.C. Choi, C.F. Lin, A modified fixed staining method for the simultaneous measurement of reactive oxygen species and oxidative responses, Biochem. Biophys. Res. Commun. 430 (2013) 442–447.
[47] W. Yu, M. Ye, J. Zhu, Y. Wang, C. Liang, J. Tang, H. Tao, Y. Shen, Zinc phthalocyanine encapsulated in polymer micelles as a potent photosensitizer for the photodynamic therapy of osteosarcoma, Nanomedicine 14 (4) (2018) 1099–1110.
[48] P.S. Saneesh Babu, P.M. Manu, T.J. Dhanya, P. Tapas, R.N. Meera, A. Surendran, K.A. Aneesh, S.J. Vadakkancheril, D. Ramaiah, S.A. Nair, M.R. Pillai, Bis(3,5-diiodo-2,4,6-trihydroxyphenyl) squaraine photodynamic therapy disrupts redox homeostasis and induce mitochondria-mediated apoptosis in human breast cancer cells, Sci. Rep. 7 (2017) 42126.
[49] A. Juarranz, J. Espada, J.C. Stockert, A. Villanueva, S. Polo, V. Verónica Domínguez, M. Cañete, Photodamage induced by zinc(II)-phthalocyanine to microtubules, actin, α-actinin and keratin of HeLa cells, Photochem. Photobiol. 73 (3) (2001) 283–289.
[50] U. Chitgupi, Y. Qin, J.F. Lovell, Targeted nanomaterials for phototherapy, Nanotheranostics 1 (1) (2017) 38–58.